

2. TOKAMAK ISTTOK

J.A.C. Cabral and C.A.F. Varandas (Heads) R. Galvão H. Fernandes, I. Nedzelskij, V. Plyusnin, C. Silva, M.P. Alonso, B.B. Carvalho, H. Figueiredo, R. Gomes, A. Soares, Y. Tashev, P. Amorim

2.1. INTRODUCTION

This project has included, besides the normal tokamak maintenance activities, work in the following main research areas:

- Testing of the liquid metal limiter concept;
- Diagnostics;
- Plasma physics studies.

2.2. TESTING OF THE LIQUID METAL LIMITER CONCEPT

2.2.1. Introduction

This research line, carried out in collaboration with the Association EURATOM/University of Latvia, had delays due to some problems on the finalization of the detailed design, testing of the injector and launching of the call for tenders.

The following main activities were performed in 2003 by IST/CFN staff:

- Collaboration on the finalization of the design of the liquid metal system (LMS) and on the definition of the technical characteristics of the LMS components;
- Development of a system to control the LMS operation;
- Development of an experimental stand to test the influence of a pulsed magnetic field on the behaviour of the liquid metal jet. The electrical circuit required to generate a 0.15 T B-field during 100 ms has been implemented and tested;
- Participation in Riga in two experimental campaigns concerning the testing of the MHD stability of the liquid gallium jet as well as the optimization of the injector;
- Organization of a workshop on the use of liquid metals in fusion research, on February 28th, at IST. This scientific meeting had 17 participants from 8 EURATOM Associations.

2.2.2. Description of the experimental set-up

The liquid metal jet is generated by hydrostatic pressure with Gallium flowing from a reservoir (Upper reservoir in Figure 2.1) placed high above (~1.3 m) the top of ISTTOK tokamak. Gallium interacting with plasmas is received at the collector, after passing through the chamber, and then transferred to the lower deposit. The procedure is repeated by pumping liquid metal from this reservoir to the upper one. For that purpose a specially designed MHD pump, based on permanent magnets and with controllable output

pressure, is used. In order to introduce Oxide-free Gallium in the loop a “cleaning system” has been designed. This setup is based on the fact that oxides have lower density than pure Gallium and therefore are deposited at the walls of the main container. Oxide-free Gallium is collected from the bulk after being degassed at high temperature (200 °C) and in UHV (10^{-7} mBar) conditions.

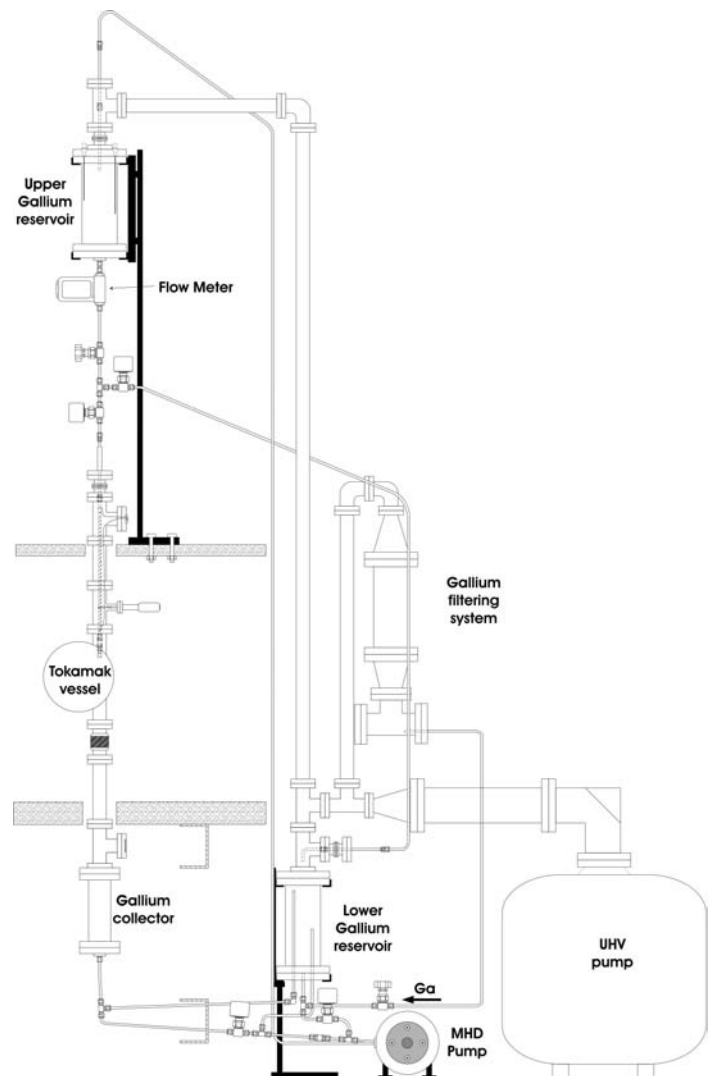


Figure 2.1 - Schematic illustration of the Ga LM loop limiter to be implemented in ISTTOK.

2.2.3. Testing of the injector

During two missions performed in Riga it has been possible to test one of the main components of the liquid metal loop: the injector. This is based on a 1/4" stainless steel pipe ended by a smaller size shaping nozzle clamped to the main tube by a special procedure. This component has been thoroughly studied and several nozzle sizes have been investigated to check both the geometrical behavior and stability. Results of these tests are shown in Figure 2.2, for several main valve opening times. Three regimes were clearly identified: (i) filling of the injector pipe after valve opening; (ii) stable jet formation; and (iii) dropping process after valve shutoff. The tests have shown that a 2.2 mm nozzle diameter would be preferable, for the operation in ISTTOK, in order to achieve a 14 cm continuous jet body (the liquid jet spontaneously decomposes into droplets due to Rayleigh instability). This requirement ensures that no Gallium droplets are interacting with the plasma.

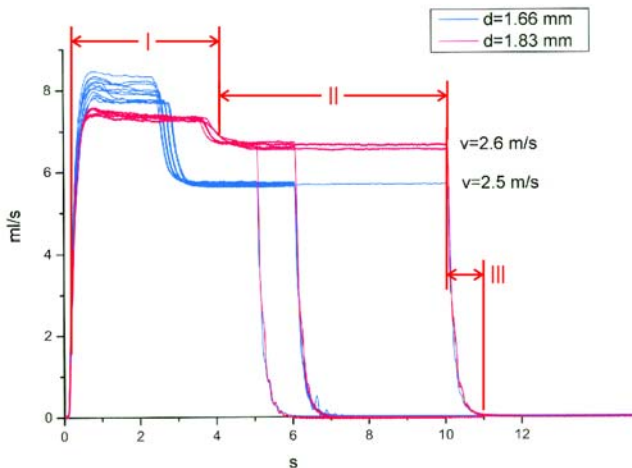


Figure 2.2 - Liquid metal flow for 1.66 and 1.83 mm nozzle diameter. I: filling phase, II: stable jet phase, III droplet formation phase.

2.3. DIAGNOSTICS

2.3.1. Main activities

The following main activities were made in 2003:

- Continuation of the development of a new spectrometer devoted to the analyses of Gallium spectral lines¹. An optical objective, required to gather the light emitted from the Gallium species (neutral+ions) and to introduce it in the spectrometer (by fiber optics) has been designed and assembled. The software necessary to control this apparatus and the CCD camera that will perform the radiation detection has been developed and

¹Work in collaboration with the Association EURATOM/ University of Latvia.

successfully tested. Figure 2.3 shows a typical plasma spectrum in the CIII region.

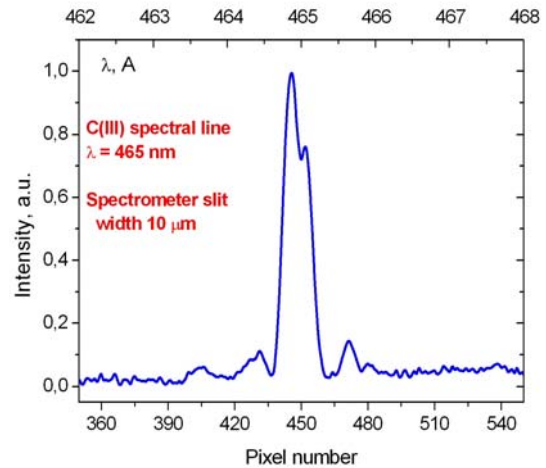


Figure 2.3 - ISTTOK plasma spectrum in the CIII region.

- Implementation of a new arrangement of three emissive probes and one cold probe for the study of Reynolds stress and the radial fluctuation-induced flux in the ISTTOK edge region;
- Improvements on the operation software of the diagnostic real-time for plasma control and on the numerical codes for the analysis of the plasma equilibrium
- Development, testing and implementation of a new time-of-flight energy analyzer (TOFEA) prototype with cylindrical electrostatic plates, together with switched power supplies for driving the TOFEA electrostatic plates. Plasma signals have been obtained on the "start" and "stop" detectors in modulation mode of HIBD operation with frequencies up to 100 kHz.
- Development of a new diagnostic for the monitoring of the C^{III} spectral line;
- Repair of the laser of the Thomson scattering diagnostic. Design of a new cooling system. Design of a new beam delivery system taking into account the new constraints imposed by the implementation on ISTTOK of the liquid metal limiter system. Development of new hardware and software for the link of the dedicated data acquisition system of this diagnostic to the central ISTTOK system;
- Beginning of the conceptual design of a multi-fiber Thomson scattering diagnostic;
- Implementation of a Gunderstrup probe provided by IPP-Prague.
- Design and implementation of an emissive electrode for biasing experiments

2.3.2. Gunderstrup probe

This probe consists of eight conducting segments mounted around an insulating cylindrical housing in order to measure the polar diagram of the ion saturation current.

Figure 2.4 shows an example of the ion saturation current polar plots measured by the Gunderstrup probe (located at $r=6.8$ cm) for positive (80 V), negative (-200 V) and no limiter bias. The parallel and perpendicular directions are indicated in the figure. It is clear that the modification in the perpendicular Mach number is in opposite directions for positive and negative bias. Both the direction and the magnitude of the estimated radial electric field are in good agreement with the rake probe data.

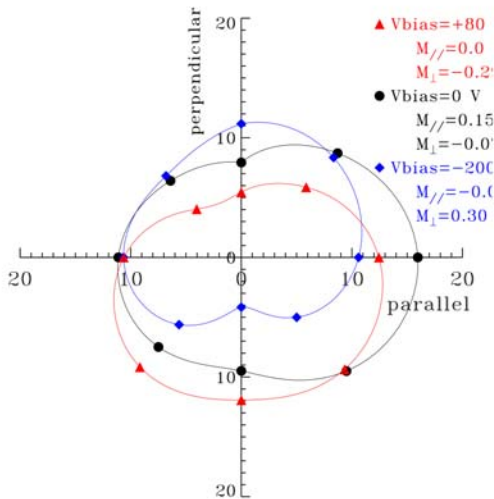


Figure 2.4 - Polar plot of the ion saturation current (mA) measured by the Gunderstrup probe for positive ($V_{bias}=80$ V), negative ($V_{bias}=-200$ V) and no limiter bias for $r_{lim}=6.2$ cm.

2.3.3. Emissive probes

Figure 2.5 presents the new setup of probes used to determine simultaneously the radial and poloidal electric fields and its fluctuations (by the emissive probes) as well as the ion saturation current (by the cylindrical cold probe). Each of the emissive probes used in our arrangement consists of a ceramic tube (Al_2O_3) with a circular cross-section of 2.8 mm outer diameter and a length of a few cm. Each Al_2O_3 tube has four bores of 0.5 mm diameter each, through which a 0.2 mm diameter tungsten wire is inserted in such a way that on one side of the tube (at the "hot end") a tungsten wire loop of an approximate total length of 6 mm is formed. Inside the bores, the tungsten wire extends at least 3 cm towards the other end (the "cold end") of the ceramic tube. Before the insertion, each tungsten wire is spliced twice with about 18 to 20 copper threads with diameters of 0.05 mm. In this way, inside the bores the tungsten wires are densely covered with a layer of Cu so that the conductivity of these parts is increased.

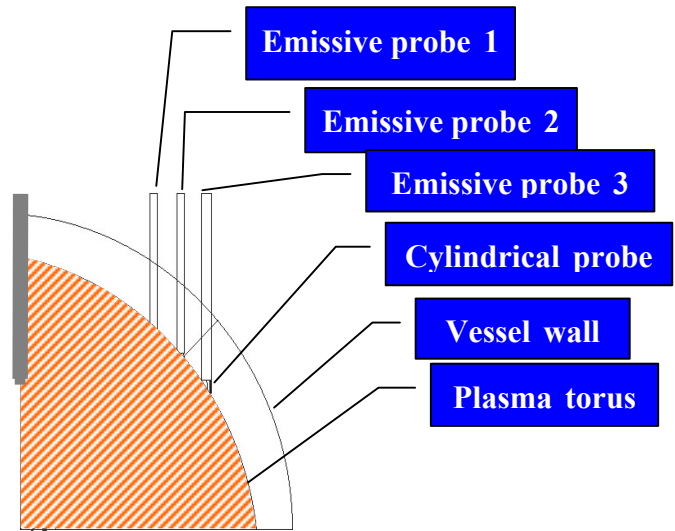


Figure 2.5 – Schematic drawing of the new probe set-up

The wrapping of the tungsten wires with Cu-threads is carried out in such a way that the electrical and mechanical contact between the tungsten and the copper is optimized. This is further enhanced by the roughness of the tungsten wire and the softness of the copper. By careful choice of the number of Cu-threads by which the tungsten wire is wrapped, the thickness of the combined wire can be adjusted so that it tightly fits into the bores of the Al_2O_3 tube. This provides an excellent electrical and mechanical contact between the two materials, which can otherwise not be soldered or welded together. On the cold end of each tube, only the spliced Cu-wires are protruding and can there be connected easily to any further electrical lead.

This construction has the effect that only the exposed loop of each emissive probe is heated when a current is passed through the probe wire. The total resistance of such a probe is about 0.11Ω . Each probe is heated by an independent battery-powered power supply with currents up to 7.5 A. Normal lead batteries are used in order to avoid ground loops and 50 (or 60 Hz) noise. In order to maximize the life times of the probe wires, the probe heating currents were only turned on a few seconds before each shot and were kept constant until the end of the discharge. The wires attained temperatures of about 2900 K. Figure 2.6 shows one of the electronic circuits for probe heating.

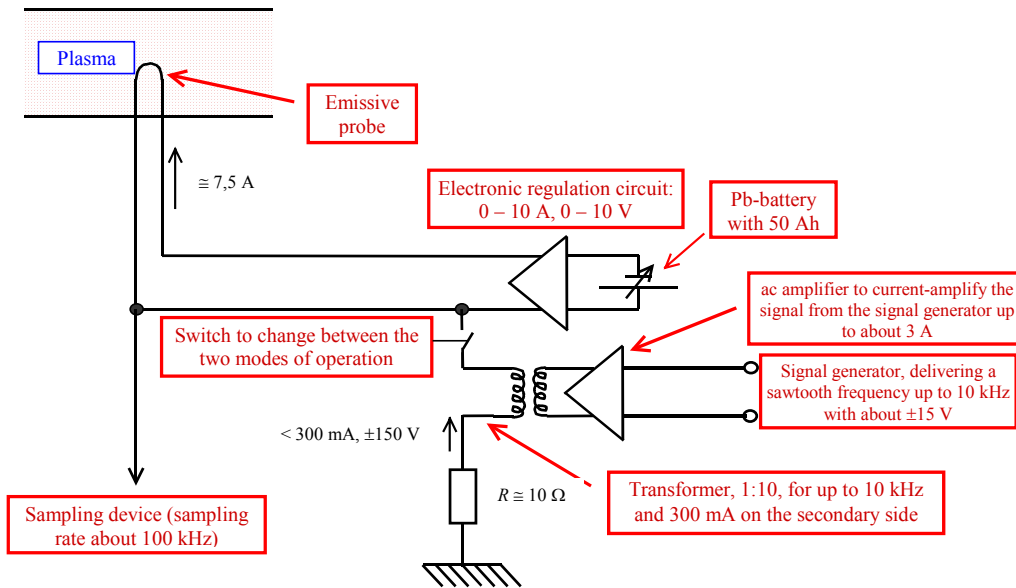


Figure 2.6 - Battery-powered electronic circuit for heating one of the emissive probes. The electric power is delivered by a simple lead battery to avoid ground loops and 50 (or 60 Hz) noise.

2.3.4 Electron emissive electrode for plasma biasing experiments

A technique used for external modification of the radial electric field in fusion plasma devices consists in biasing of plasma facing components, like limiters, or inserting biased electrodes into the edge plasma. In small tokamaks with relatively low plasma density, the current collected by negative biased standard electrodes is not sufficient to decrease the plasma potential due to the limitation imposed by the ion saturation current. Emissive electrodes produce a much larger current, therefore allowing a more efficient way to control the edge radial electric field.

A movable emissive electrode has been developed for the biasing experiments in ISTTOK. The bias circuit is

presented in figure 2.7a and the electrode head is depicted schematically in figure 2.7b. The emissive electrode consists of a LaB₆ (Lanthanum Hexaboride) disk with a diameter of 16 mm and covered by a Tantalum cylinder, which is protected by Boron Nitride cup as insulating material to be exposed to the plasma. This type of cathodes is generally applied in electron guns and characterized by low (2.69 eV) work function, high (2210° C) melting point and stability at high temperatures, low vapor pressure, chemical stability and high (ten times higher than tungsten) brightness. Up to 30 A of steady state current can be emitted along the magnetic field, returning to the wall by cross-field transport.

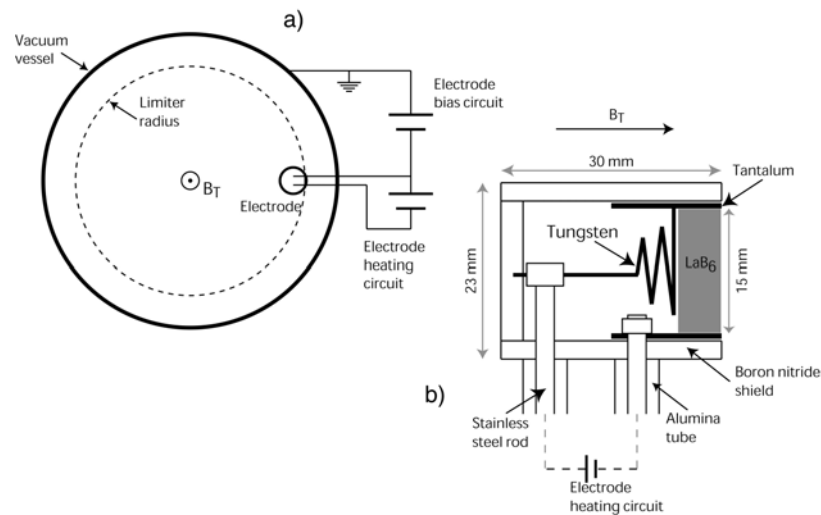


Figure 2.7 - Schematic drawing of the bias and heating circuits (a) and the emissive electrode (b).

It has been found that the emitted current, I_{em} , increases with the emitter temperature in rough agreement with the Richardson-Dushman formula, which is characterized by an approximately zero current up to a threshold electrode temperature (approximately 1700°K) and then a fast current increase above that value. The current-to-voltage characteristic of the emissive electrode has been investigated in a simple vacuum diode configuration and in plasmas. The IV characteristic in vacuum is well described by Child-Langmuir law. However, that is not the case in the plasma. Figure 2.8 shows the I-V characteristics obtained during AC (sinusoidal, ± 120 V, 50 Hz) and DC (2 ms pulses with a 10 μ s rise time) biasing of cold and heated emissive electrode, when operating in the ISTTOK plasma. The dependence of the emitted current in plasma (which is the difference between the currents of hot and cold electrode) is clearly different from that in the diode configuration: the current value is much larger, and a tendency to saturation is observed. Replacing in Child-Langmuir law the extraction gap width by the plasma sheath thickness, a current of the same order of magnitude as observed in plasma is estimated. However, the Child-Langmuir law modification cannot explain the saturation tendency.

The emissive electrode proved to be a valuable tool on the control of the plasma electric field, allowing a detailed investigation of its importance in plasma confinement. Apart from the biasing experiments, the emissive electrode is routinely used for the gas pre-ionization in cleaning discharges of ISTTOK. The recommended vacuum for the LaB₆ cathodes operation is below 10⁻⁶ mBar for a long-life condition. During cleaning discharges and plasma shots the ISTTOK pressure rises up to 10⁻⁴ mBar. However, no clear degradation of the electrode emissive capability has been observed during the half-year of operation.

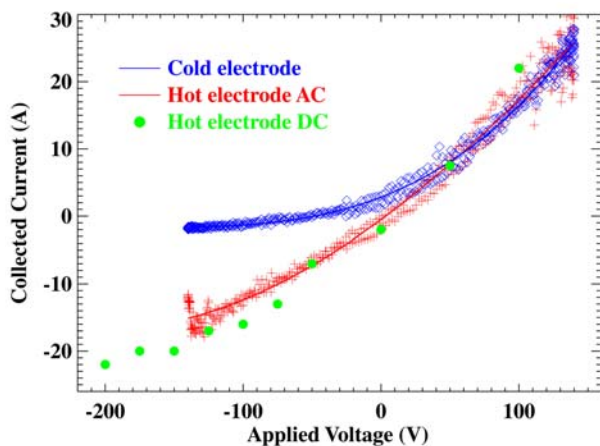


Figure 2.8 - Cold and hot IV characteristic of the electrode.

2.4. PLASMA PHYSICS STUDIES

2.4.1. Introduction

This research line has included studies related with:

- Plasma column macroscopic oscillations;
- Emissive electrode and limiter biasing experiments;
- Fluctuation and Reynolds stress measurements.

2.4.2. Non-linear model for the plasma column macroscopic oscillations

A non-linear model for the plasma column macroscopic oscillations in the tokamak ISTTOK was developed. The model is able to reproduce the main qualitative features of the oscillations seen in the experimental data. In particular, the clear phase differences observed between the current and density oscillations. The evolution of the main plasma parameters is in good qualitative agreement with the experimental data. The stability analysis of the non-linear cycle shows that stable oscillations require a large fraction of radiation losses.

The model was applied to plasma discharges, where the current in the poloidal magnetic field coils that produce the equilibrium vertical magnetic field is low ($I_{vert} \sim 120$ A) and insufficient to balance the plasma column. In these discharges, typical oscillations in the plasma current are observed. In discharge #10774, analysed in detail, the plasma current varies from the higher value of 6 kA to the lower value of 1 kA as shown in figure 2.9. The period of the oscillations is around 10ms, which allows 3-4 oscillations during a typical plasma ISTTOK discharge of 30-40ms. During the initial phase of the discharge as the current increases the plasma moves outwards due to insufficient inward force provided by the vertical magnetic field (Figure 2.10). Limited by the outside limiter the plasma current starts to decrease and an inward movement is then observed until the plasma is again limited by the inside part of the vessel.

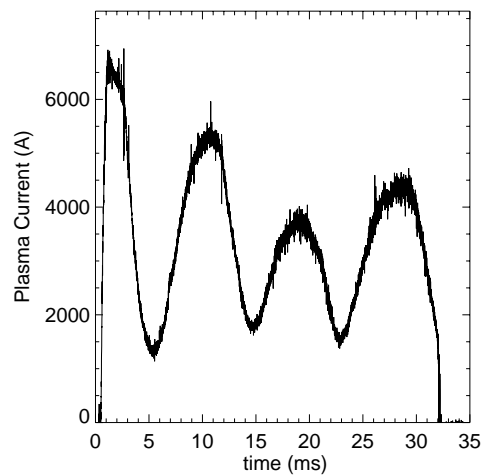


Figure 2.9 - Plasma current as a function of time, showing the typical plasma oscillations common in some discharges.

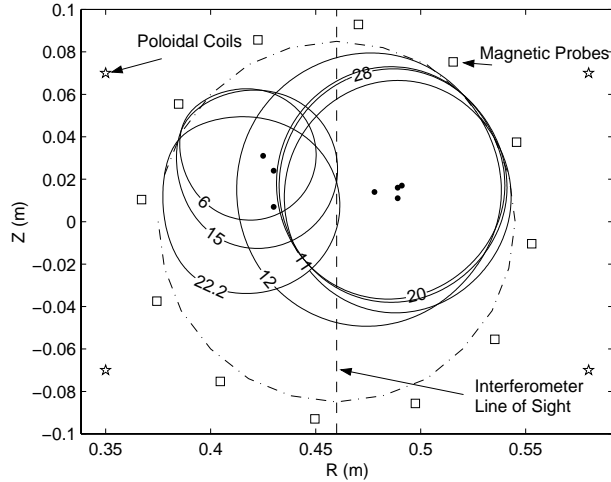


Figure 2.10 - Plasma position, reconstructed using the poloidal array of magnetic sensors and the current filament numerical approximation during the various stages of the cycle ($t=6.0$ ms, $t=11.0$ ms, $t=12.0$ ms, $t=15.0$ ms, $t=20.0$ ms, $t=22.2$ ms, $t=28$ ms) for the ISTTOK discharge #10774.

2.4.3. Emissive electrode and limiter biasing experiments²

In previous experiments performed on ISTTOK no modification in the plasma parameters have been obtained for negative electrode or limiter bias due to the low current drawn by the electrode/limiter. In order to obtain the larger current necessary to modify confinement at negative applied voltages, two different approaches have been followed in biasing experiments: (i) use of a small limiter, inserted deep inside the main limiter radius and (ii) use of a small emissive electrode made of LaB₆.

Limiter biasing experiments were the first to be performed and the results showed that, in spite of the strong perturbation of the discharge introduced by the limiter due to its large area, confinement improvement could be obtained for both polarities. It has been observed that the current collected by the limiter increases as the limiter is inserted into the plasma and that the modification in the floating potential is proportional to the collected current, suggesting that the electric field created at the edge plasma is a result of an increase in the plasma rotation due to the collected radial current. Larger electric fields are induced in the region just inside the limiter for both polarities explaining the observed improvement in confinement.

The first experimental results of edge polarization experiments with emissive electrodes, carried out in ISTTOK, have been obtained. We have shown that the edge plasma potential can be modified for both polarities in opposition to that observed with non-emissive electrodes. Furthermore, an improvement on particle confinement is

clearly observed for negative EEB. The time evolution of the main plasma parameters for a discharge with negative emissive electrode bias, $V_{\text{bias}}=-200$ V is presented in figure 2.11. As the bias is applied, the floating potential at the plasma edge is modified in a rather short time scale (<50 μ s), the bias current amplitude increases rapidly to a maximum value, around 20 A, and it starts to present a sawtooth behavior. The floating potential decreases by about 60 V, at $r-a=-6$ mm, while close to the limiter it does not change significantly, leading to a strong modification in the edge radial electric field (from -1 to -7 kV/m) in the region just inside the limiter (figure 2.12).

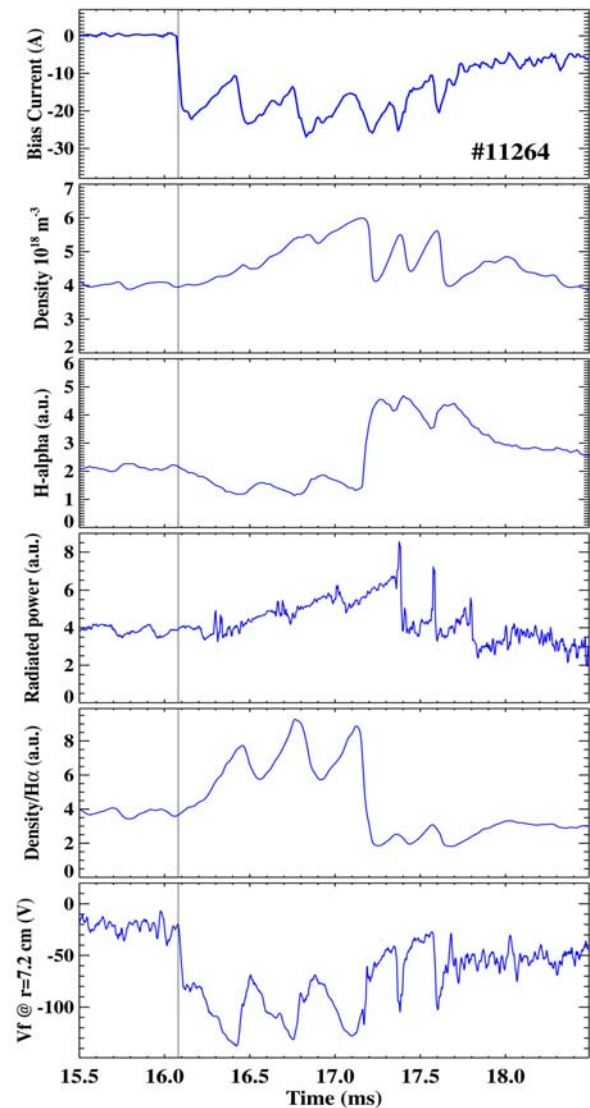


Figure 2.11 - Time evolution of the main plasma parameters for a discharge with negative emissive electrode bias ($V_{\text{bias}} = -200$ V). The bias voltage was applied at $t \approx 16$ ms for 4 ms.

² Work in collaboration with the University of Gent, Institute of Plasma Physics – Prague and “Instituto de Fisica da Universidade de Sao Paulo”.

In spite of the oscillations observed in the emission current, the line-averaged density increases substantially, $\Delta\bar{n}/\bar{n} \approx 50\%$. The radiation losses are also observed to increase, being the rise roughly proportional to that observed in the density, so that there is no evidence for significant impurity influx during the bias. Furthermore, since the H_α radiation intensity decreases significantly, $\Delta I_{H_\alpha}/I_{H_\alpha} \approx -40\%$, after the bias is applied, there is clear indication of a reduction in recycling. The gross global particle confinement time, τ_p , almost doubles at the peak of the oscillations, as inferred from the ratio \bar{n}/H_α .

The main result of these experiments is the discovery of improved confinement events (ICEs), which are characterized by a steady increase of the plasma density associated with a decrease of the H_α radiation. These events are observed for both negative and positive bias, provided that the bias current is larger than a threshold value, $|I_{\text{bias}}| \approx 20$ A. As the polarization voltage is increased, the bias current starts to increase linearly with the radial electric field and reaches a saturation value, after which it decreases. In some cases, the radial profile of the radial electric field shows a double-peaked structure at the beginning of an ICE, and later relaxes to a single peaked structure, as the density increases towards its maximum during the event.

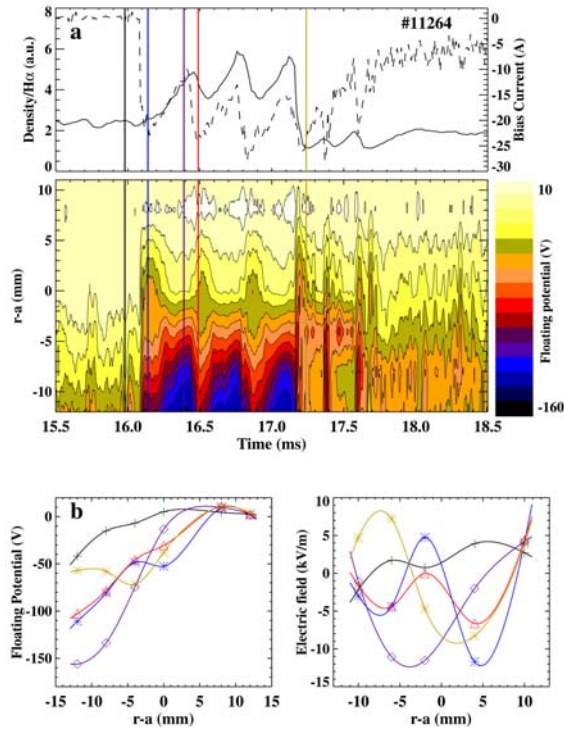


Figure 2.12 - (a) Time evolution of the collected current, ratio \bar{n}/H_α and floating potential radial profiles for a discharge with emissive electrode bias. (b) Radial profiles of the floating potential and radial electric field for the times indicated in (a).

2.4.4. Effect of limiter position

The influence of the position of a localized limiter (a section of a poloidal limiter covering a poloidal extension of 90°) on the plasma biasing efficiency has been investigated in detail. For $r_{\text{lim}} > 6.7$ cm, both the edge and main plasma parameters do not change significantly as the limiter is inserted into the plasma. However, this is clearly not the case for $r_{\text{lim}} < 6.7$ cm where a reduction in both the average plasma density and the H_α radiation are observed, associated with a significant modification of the edge floating potential profile. Furthermore, measurements of the limiter short-circuit current (SC-current) variation with limiter position allowed the identification of two distinct zones, which are characterized by a change in the SC-current sign at the vicinity of $r_{\text{lim}} \sim 7.2$ cm.

The SC-current has also been measured during the electrode bias experiments. As the limiter is inserted into the plasma, the fraction of the bias return current collected by the limiter strongly increases, indicating that the plasma becomes detached from the wall. These results explain the increase of the electrode IV characteristic symmetry as the limiter is inserted into the plasma. As the plasma becomes detached from the wall the latter cannot provide the return current required by large positive bias. The increase of the ion current as the limiter is inserted is therefore much larger than that observed for the electron current.

The effect of bias on the plasma parameters is also clearly influenced by the limiter position. As the limiter is inserted into the plasma, both the collected current and the modification of the floating potential induced by bias increases slowly up to $r_{\text{lim}} = 6.7$ cm, rising then much faster up to $r_{\text{lim}} = 6.2$ cm. Based on these results two zones of limiter position may be identified in relation to the properties of non-biased and biased plasmas. For clarity, we name these zones as Far-zone and Close-zone for $6.7 \text{ cm} < r_{\text{lim}} < 7.8 \text{ cm}$ and $r_{\text{lim}} < 6.7 \text{ cm}$, respectively.

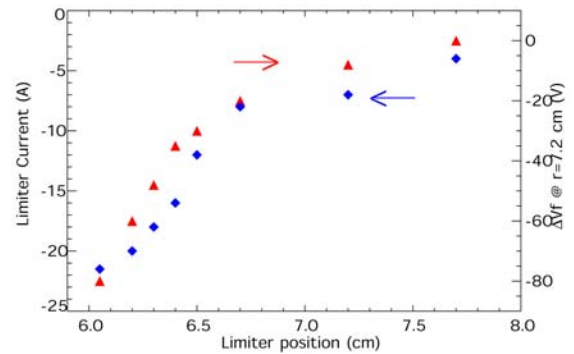


Figure 2.13 - Variation of the limiter current and modification in the floating potential (ΔV_f) at $r=7.2$ cm with the limiter position at constant applied voltage ($V_{\text{bias}} = -200V$)

	Far-zone	Close-zone
Non-biased plasma	1. Mostly positive (ion) non-ambipolar flow to the limiter. 2. Modest change of edge plasma parameters with variation of limiter position inside zone.	1. Mostly negative (electron) non-ambipolar flow to the limiter. 2. Variation of edge plasma parameters with variation of limiter position inside zone.
Biased plasma	No or modest modifications of edge and global plasma parameters during both negative and positive biasing.	Strong modifications of edge and global plasma parameters during both negative and positive biasing.

Table 2.1 – Summary of the limiter position effects on the plasma parameters.

Naturally, it is important to consider that the boundary between the two zones is not precisely determined, because of the uncertainties in the limiter position, and the thickness of the limiter itself. The general properties of the non-biased and biased plasmas when limiter is positioned inside these zones are summarized in table 2.1.

2.4.5. Fluctuation and Reynolds stress measurements³

The fluctuations of the poloidal and radial electric field as well as of the ion density have been measured simultaneously in the edge region of the ISTTOK plasma with an arrangement of three electron-emissive probes and one cold probe. From this information, the Reynolds stress (R_e) and the fluctuation-induced flux (Γ) have been calculated.

Figure 2.14 shows radial profiles of Γ (red solid line), R_e (blue dashed line) and of dR_e/dr (black dotted line) in the ISTTOK edge region, determined on a shot-to-shot basis. The vertical line indicates the position of the last closed flux surface (LCFS). It is interesting to note that near the LCFS, the radial gradient of R_e reaches a maximum near the minimum of Γ . This corroborates the model that a large radial gradient of R_e produces a sheared poloidal flow, which reduces the radial transport.

Figure 2.15 shows the probability distribution function (PDF) of the Reynolds stress at the radial position of 72 mm, while the shear layer was at 82 mm. When the three probes were unheated (blue curve) the cold probe floating potentials V_{fl} were used as approximations for the plasma potentials.

Once the probes were heated to electron emission (red curve) a better approximation of the plasma potential was used as a basis for calculating R_e . The PDF determined with the emissive probes is narrower but it also shows a more non-Gaussian character than that determined with the cold probes. Temperature fluctuations are probably the cause for this difference as they are ignored when cold probe are used.

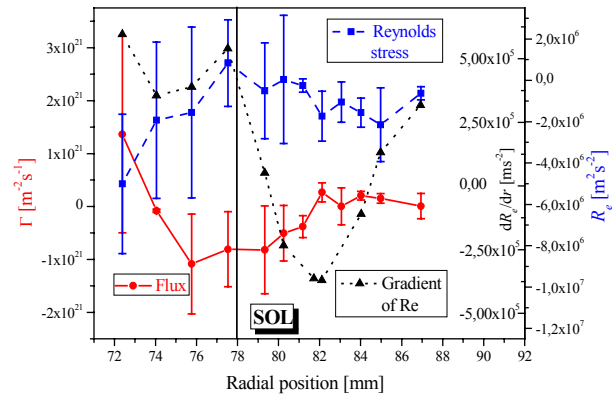


Figure 2.14 - (a) Time evolution of the collected current, ratio \bar{n}/H_α and floating potential radial profiles for a discharge with emissive electrode bias. (b) Radial profiles of the floating potential and radial electric filed for the times indicated in (a).

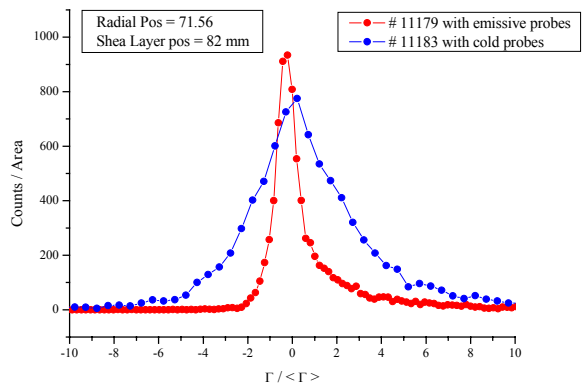


Figure 2.15 - Probability distribution function (PDF) of the Reynolds stress at $r \cong 72$ mm, once determined by the three probes unheated (blue) and once heated (red). The latter case should give the more reliable result.

³Work in collaboration with the University of Innsbruck.